Supplemental Information

2D Metal-Organic Frameworks derived Co/$CoSe_2$ heterojunction with interfacial electron redistribution as bifunctional electrocatalysts for Urea-assisted rechargeable Zn-air batteries

Huanhuan Li [a], Yanyan Liu [a, *], Lulu Huang [a], Jie Xin [a], Tengfei Zhang [a], Ping Liu [a], Long Chen [a], Wen Guo [a], Tiantian Gu [a], Gang Wang [a, b, *]

[a] School of Chemistry and Chemical Engineering, State Key Laboratory Incubation Base for Green Processing of Chemical Engineering, Shihezi University, Shihezi 832003, P. R. China

[b] Key Laboratory of Materials-Oriented Chemical Engineering of Xinjiang Uygur Autonomous Region, Shihezi 832003, P. R. China

* Corresponding authors at: School of Chemistry and Chemical Engineering, State Key Laboratory Incubation Base for Green Processing of Chemical Engineering, Shihezi University, Shihezi 832003, PR China (G. Wang).

E-mail addresses:

liuyy_jobmail@163.com (Y. Liu),

wanggang@shzu.edu.cn (G. Wang).

1. Experimental

1.1 Chemical and materials

$Co(NO_3)_2 \cdot 6H_2O$, $Zn(NO_3)_2 \cdot 6H_2O$, 2-methylimidazole (2-MIM), melamine and cyanuric acid were all purchased from Shanghai Macklin Reagent Factory. Commercial catalysts of Pt/C (20 wt%) and RuO_2 (99.95 wt%) were purchased from Johnson Matthey and Adamas-beta, respectively.

1.2 Synthesis of CoZn-ZIF

$Zn(NO_3)_2 \cdot 6H_2O$, $Co(NO_3)_2 \cdot 6H_2O$ and 2-methylimidazole (2-MIM) in a molar ratio of 1:8 were dissolved in 40 mL of deionized water, respectively. And then the aqueous solution of metal nitrate was added into the aqueous solution of 2-MIM with magnetic stirring for 2 h and kept at room temperature for 10 h. The purple precipitate was collected by centrifugation, then washed and dried.

1.3 Synthesis of CoZn-ZIF@MCA

For the preparation of CoZn-ZIF@MCA, 0.25 g of melamine was dissolved in 20 mL of dimethylsulfoxide (DMSO). Then, 0.5 g of ZIF was added into the above solution and dispersed by stirring. Subsequently, a solution of cyanuric acid (0.25 g) in 20 mL of DMSO was added under vigorous stirring for 30 min. The solid precipitate of CoZn-ZIF@MCA was rinsed several times with ethanol and then dried at 60 °C.

1.4 Synthesis of $Co/CoSe_2$@CNx

The prepared MCA@ZIF precursor was placed in a tube furnace in a nitrogen atmosphere at a heating rate of 5 °C/min to 800 °C for 2 h and naturally cooled to room temperature to obtain Co@CNx. The as-synthesized Co@CNx (100 mg) was placed at

the center of the tube furnace. The Se powder (200 mg) was placed in the upstream position in the tube furnace. The sample was then annealed at 500 °C for 2 h with a heating rate of 2 °C/min under a nitrogen atmosphere, followed by cooling to room temperature naturally, and the Co/$CoSe_2$@CNx were successfully prepared. As a comparison, a similar synthetic process was used to fabricate $CoSe_2$@CNx composites to highlight the synergistic effect of heterojunctions, where only Co and Se powders were changed to 1:10 by mass ratio.

1.5 Structural characterization

The crystal structure of samples was confirmed by powder X-ray diffraction (PXRD) patterns on a Rigaku Ultima IV with Cu-Kα radiation. The scanning electron microscopy (SEM) was obtained by using a Zeiss Sigma 300 scanning electron microanalyzer. The transmission electron microscopy (TEM) and high-resolution TEM (HRTEM) and elemental mappings were collected on a F200X field emission TEM at 200 kV. The chemical compositions of the samples were determined by X-ray photoelectron spectroscopy (XPS) on a Thermo Scientific K-Alpha X-ray photoelectron spectrometer with the Mg Kα X-ray as the excitation source. The specific surface areas and corresponding pore size distributions were measured at 77 K with Micromeritics ASAP 2460 by the method of nitrogen adsorption-desorption isotherms.

1.6 Electrochemical measurements

The tests of electrocatalysts were evaluated with a three-electrode system, where glassy carbon rotating disk electrode (GC RDE, 0.19625 cm^{-2}), Ag/AgCl electrode and

platinum wire serve as the working, counter and reference electrodes, respectively. The ink containing 4 mg of electrocatalyst, 900 μL of ethanol and 100 μL of 5% Nafion solution was loaded onto the GC RDE and dried for further tests.

The ORR performance of the samples was evaluated by cyclic voltammetry (CV) and linear sweep voltammetry (LSV) measured in 0.1 M KOH electrolyte, and the UOR and OER performance were evaluated in 1.0 M KOH solution with or without 0.33 M urea. The bifunctional activity of catalysts is estimated by the potential difference (ΔE) between ORR and UOR:

$$\Delta E = UOR_{Ej10} - ORR_{E1/2}$$

where UOR_{Ej10} is the potential at a current density of 10 mA cm^{-2} for UOR, and $ORR_{E1/2}$ is the half-wave potential for ORR.

1.7 Zinc-air battery tests

To evaluate the comprehensive performance of the catalyst, an electrochemical cell was used to assemble the urea-assisted rechargeable ZABs. Aqueous Zn-air batteries were assembled and tested in the alkaline electrolyte composed of 6 M KOH, 0.2 M $Zn(CH_3COO)_2$ and 0.33 M urea. The air cathode was prepared by uniformly loading the prepared $Co/CoSe_2$@CNx catalyst on a carbon paper (~1 mg cm^{-2}) and a gas diffusion layer was attached to the other side of the Nickel foam. A polished Zn functioned as the anode. As a comparison, the conventional zinc-air battery was assembled using a mixture of 6 M KOH and 0.2 M $Zn(Ac)_2$ solution.

1.8 Working mechanism of conventional rechargeable ZABs

Charging process:

OER at cathode (6 M KOH + 0.2 M $Zn(CH_3COO)_2$):

$4OH^- - 4e^- \rightarrow 2H_2O + O_2$ (E = 0.40 V *vs*. SHE) (S1)

Zinc deposition at anode (6 M KOH + 0.2 M $Zn(CH_3COO)_2$):

$ZnO + 2OH^- + H_2O \rightarrow Zn(OH)_4^{2-}$

$Zn(OH)_4^{2-} + 2e^- \rightarrow Zn + 2OH^-$

$Zn^{2+} + 2e^- \rightarrow Zn$ (E = -1.25 V *vs*. SHE) (S2)

Overall reaction:

$2ZnO \rightarrow 2Zn + O_2$ E= 1.65 V (S3)

Discharging process:

ORR at cathode (6 M KOH + 0.2 M $Zn(CH_3COO)_2$):

$O_2 + 4e^- + 2H_2O \rightarrow 4OH^-$ (E = 0.4 V *vs*. SHE) (S4)

Zinc dissolution at anode (4 M KOH + 0.1 M $Zn(CH_3COO)_2$):

$Zn + 4OH^- \rightarrow Zn(OH)_4^{2-} + 2e-$

$Zn(OH)_4^{2-} \rightarrow ZnO + H_2O + 2OH^-$ (E = –1.25 V *vs*. SHE) (S5)

Overall reaction:

$2Zn + O_2 \rightarrow 2ZnO$ (E = 1.65 V) (S6)

1.9 Working mechanism of urea-assisted rechargeable ZABs

Charging process:

UOR at cathode (6 M KOH + 0.33 M urea):

$CO(NH_2)_2 + 6OH^- \rightarrow CO_2 + N_2 + 5H_2O + 6e^-$ (E= -0.37 V *vs*. SHE) (S7)

Zinc deposition at anode (6 M KOH + 0.2 M $Zn(CH_3COO)_2$):

$ZnO + H_2O + 2e^- \rightarrow Zn + 2OH^-$ (E = –1.25 V *vs*. SHE) (S8)

Overall reaction:

$CO(NH_2)_2 + 3ZnO \rightarrow CO_2 + N_2 + 3Zn + 2H_2O$ E' = 0.88 V (S9)

Discharging process:

The discharging processes are the same as those described in Equation S4-S6.

According to the above calculations, once UOR replaces OER on cathode, the theoretical charging voltage of ZABs significantly decreases to 0.88 V, suggesting that the as-proposed urea-assisted rechargeable ZABs has theoretically a higher energy conversion efficiency.

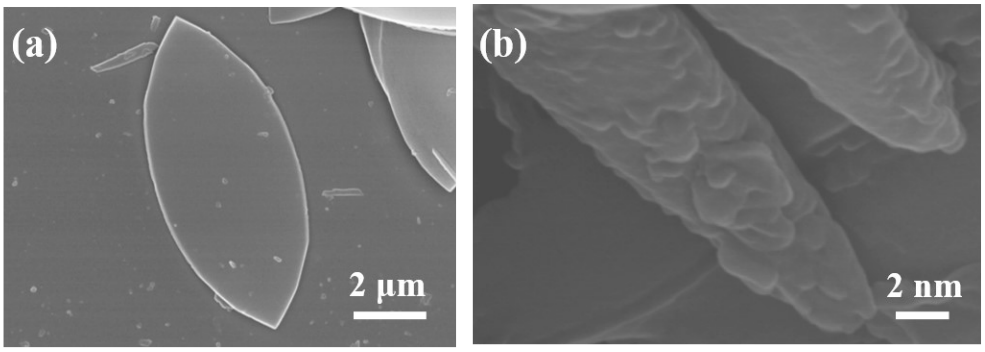

Figure S1. (a) SEM image of CoZn-ZIF-L sample (b) SEM image of CoZn-ZIF-L@MCA sample.

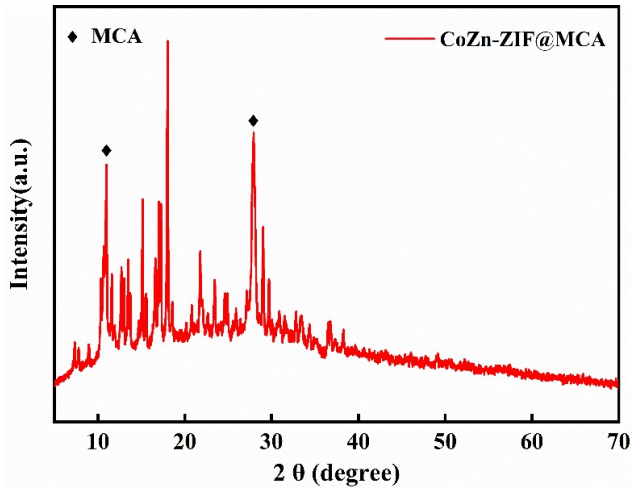

Figure S2. XRD pattern of the as-prepared CoZn-ZIF-L@MCA sample.

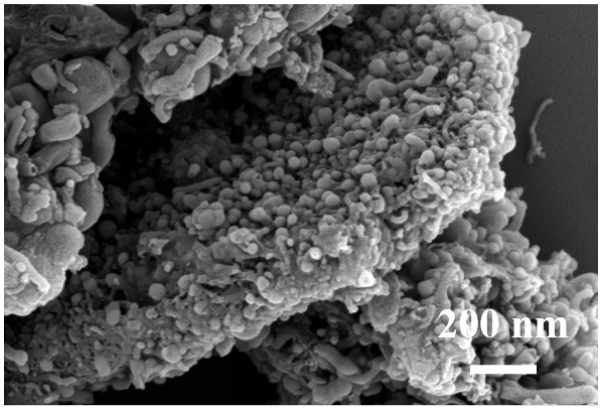

Figure S3. SEM image of Co/$CoSe_2$@CNx sample.

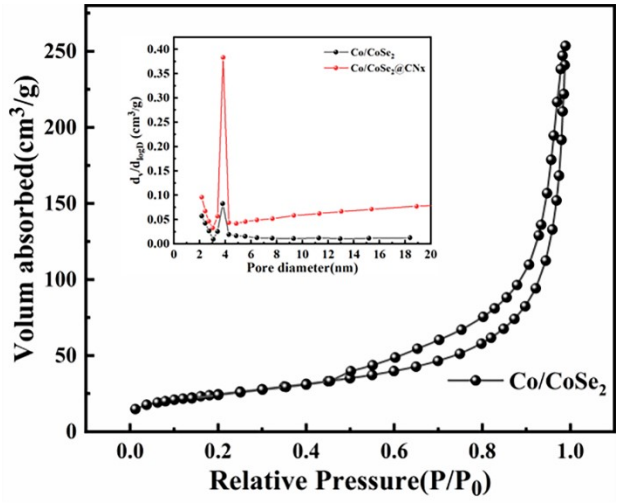

Figure S4. BET of the as-prepared $Co/CoSe_2$.

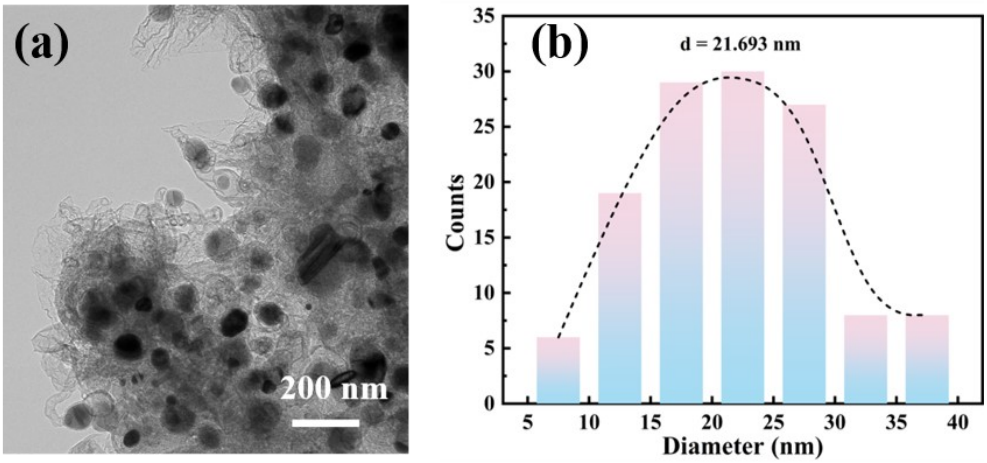

Figure S5. (a) TEM image of $Co/CoSe_2$@CNx and (b) the corresponding diameter distribution of nanoparticles.

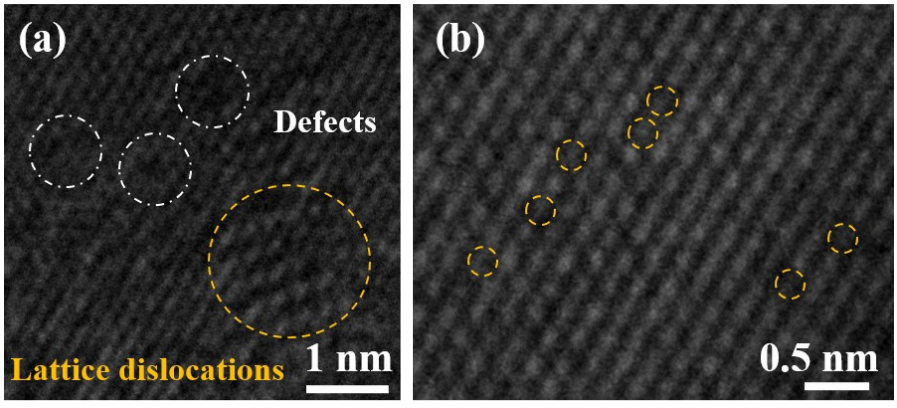

Figure S6. (a-b) Atomic-resolution HAADF-STEM image of $Co/CoSe_2$@CNx.

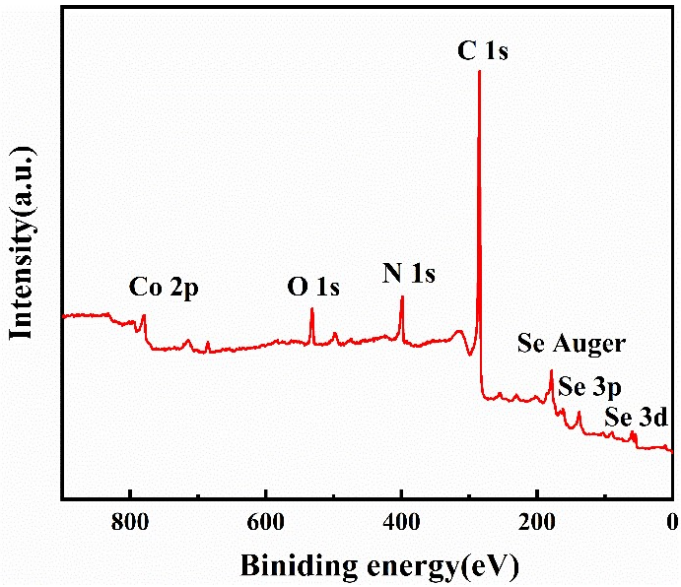

Figure S7. XPS survey spectrum of Co/$CoSe_2$@CNx.

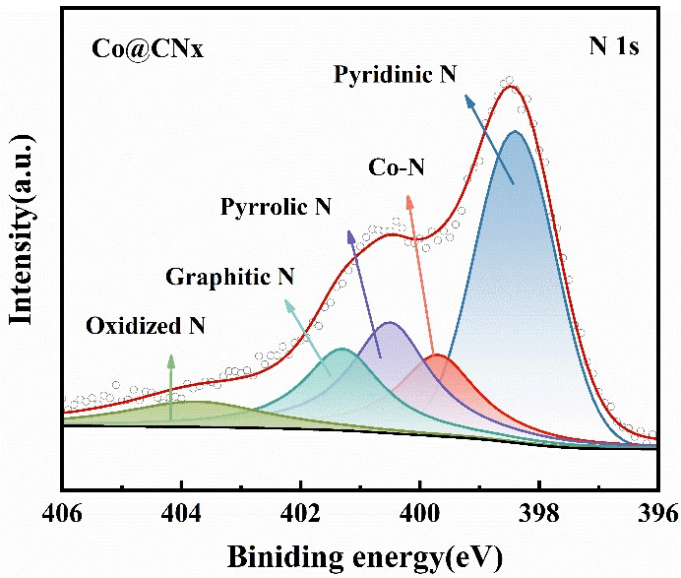

Figure S8. N 1s of Co@CNx.

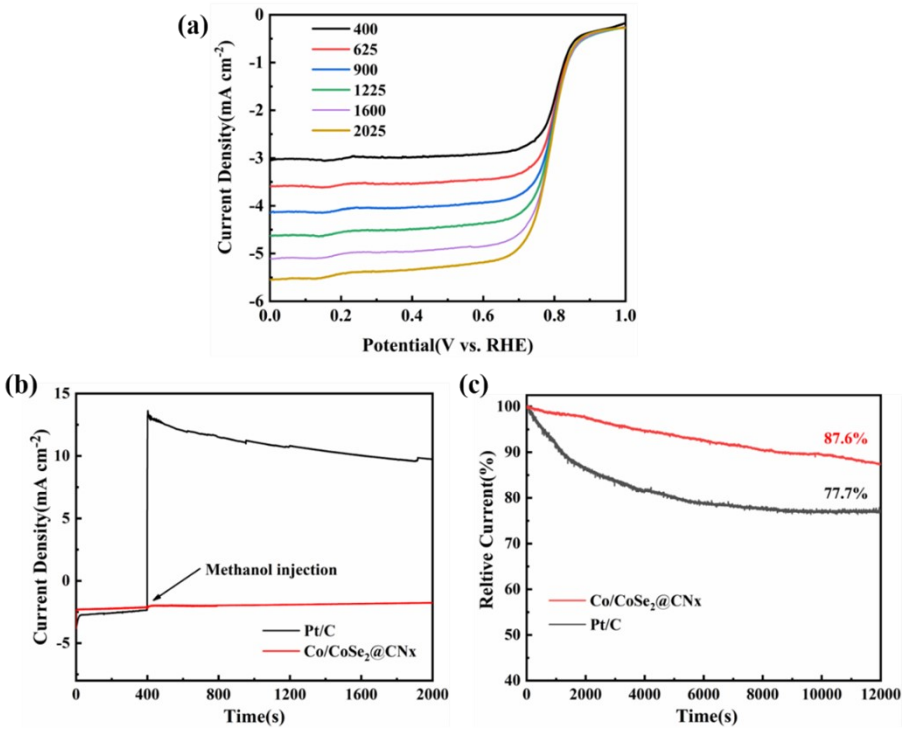

Figure S9. (a) LSV curves of Co/$CoSe_2$@CNx at different rotation speeds; (b) Methanol resistance test in 0.1 M KOH electrolyte at 900 rpm; (c) stability curves of Co/$CoSe_2$@CNx and Pt/C.

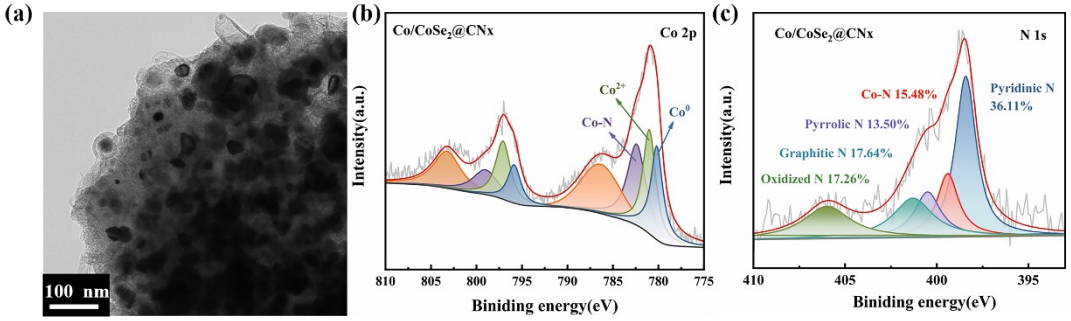

Figure S10. (a) TEM image of Co/$CoSe_2$@CNx after stability test; (b) XPS of Co/$CoSe_2$@CNx after stability test.

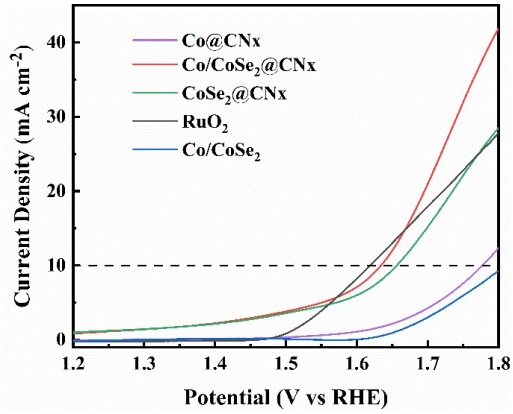

Figure S11. LSV curves of Co/$CoSe_2$@CNx, Co@CNx, $CoSe_2$@CNx, Co/$CoSe_2$ and RuO_2 (0.1M KOH, 1600rpm).

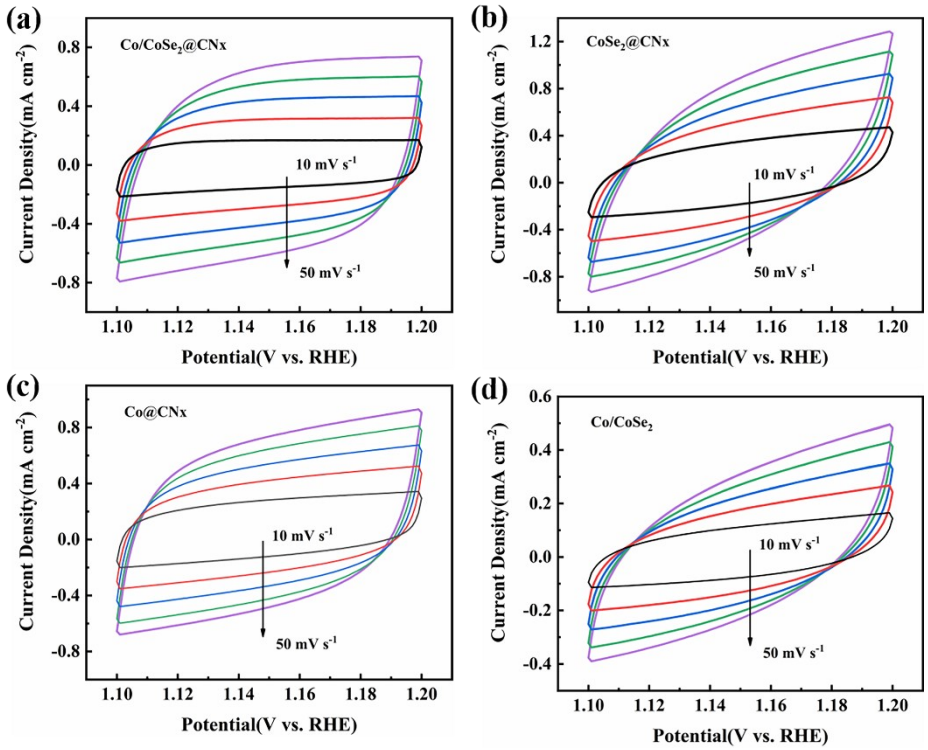

Figure S12. Electrochemical double-layer capacitance measurements at different scan rate (10, 20, 30, 40, 50 mV s^{-1}) in 0.1 M KOH. CVs of the as-prepared (a) $Co/CoSe_2$@CNx, (b) $CoSe_2$@CNx, (c) Co @CNx and (d) $Co/CoSe_2$ catalysts.

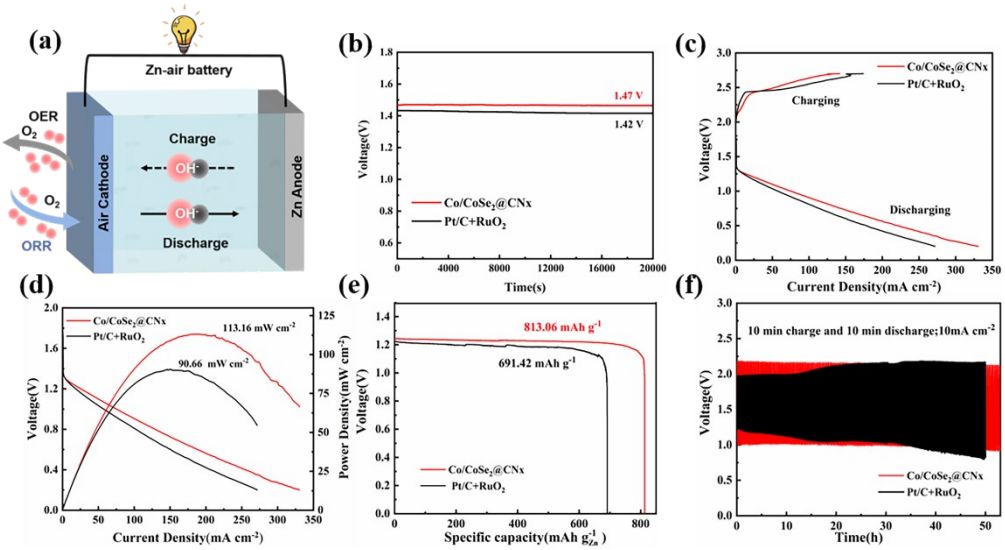

Figure S13. (a) The basic structure of ZABs; (b) The open-circuit voltage curves of ZABs based on $Co/CoSe_2$@CNx and $Pt+RuO_2$; (c) Charge and discharge polarization curves; (d) discharging polarization curves and the corresponding power density plots (e) Specific capacity curves at 10 mA cm^{-2} (f) Galvanostatic cycling stability of the ZABs at 10 mA cm^{-2}.

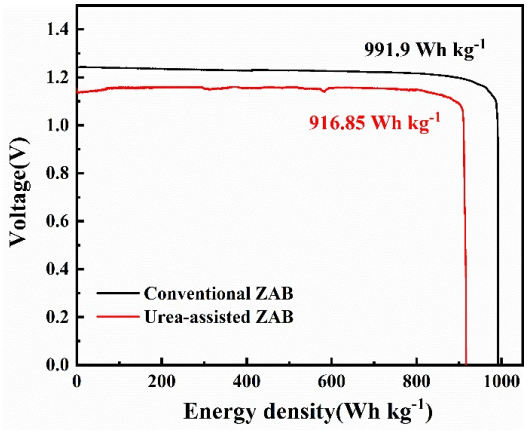

Figure S14. Energy density of urea-assisted and conventional ZABs based on Co/$CoSe_2$@CNx

Table S1. Contents of different N species in Co/$CoSe_2$@CNx and Co @CNx.

Samples	Pyridinic-N	Co-Nx	Pyrrolic-N	Graphitic-N	Oxidated-N
Co@CNx	39.96 %	15.14%	20.99 %	15.49 %	8.14%
Co/$CoSe_2$@CNx	44.52 %	15.16%	14.47 %	20.51 %	5.32 %

Table S2. Comparison of ORR activity of $Co/CoSe_2$@NC with other ORR reported metal selenide catalysts before.

Number	Catalyst	$E_{ORR1/2}$ (V)	Electrolyte	Ref.
1	$Co/CoSe_2$@CNx	0.83	0.1 M KOH	**This work**
2	$CoSe_2$/Se-rGO	0.803	0.1 M KOH	[1]
3	N-$CoSe_2$/3D $Ti_3C_2T_x$	0.79	0.1 M KOH	[2]
4	$Ni_{0.75}Mo_{0.25}OSe$	0.82	0.1 M KOH	[3]
5	FeSe@NC-900	0.80	0.1 M KOH	[4]
6	Fe-doped MOF CuCoSe@HCNFs	0.756	0.1 M KOH	[5]
7	$CoSe_2$@NC	0.83	0.1 M KOH	[6]
8	N-$NiSe_2$/CC	0.73	0.1 M KOH	[7]
9	$Ni_{0.2}Co_{0.8}Se$	0.769	0.1 M KOH	[8]
10	DBD-NiFe/ $NiSe_2$@NCNT	0.811	0.1 M KOH	[9]
11	FeSe/ NC-PoFeSe	0.81	0.1 M KOH	[10]
12	$Fe_{0.33}Sn_{0.67}OSe$	0.84	0.1 M KOH	[11]
13	Co/CoSe@NC	0.825	0.1 M KOH	[12]

Table S3. Comparison of UOR activity of $Co/CoSe_2$@NC with other UOR reported metal selenide catalysts before.

Number	Catalyst	E_{UORj10} (V)	Electrolyte	Ref.
1	$Co/CoSe_2$@CNx	1.37	1 M KOH+ 0.33 M urea	**This work**
2	$CoSe_2$@CNx	1.40	1 M KOH+ 0.33 M urea	**This work**
3	Co@CNx	1.41	1 M KOH+ 0.33 M urea	**This work**
4	Ni-S-Se/NF	1.38	1.0 M KOH +0.5 M urea	[13]
5	$NiSe_2$-NiO	1.33	1.0 M KOH +0.33 M urea	[14]
6	Fe-NiCoSe	1.458	1.0 M KOH +0.5 M urea	[15]

Table S4. Comparison of bifunctional activities of various catalysts.

Catalyst	Reactions	$E_{UOR\,j10}$ (V)	$E_{1/2}$ (V)	ΔE (V)	Ref.
$Co/CoSe_2$@CNx	ORR||UOR	1.37	0.83	0.54	**This work**
$CoSe_2$@CNx	ORR||UOR	1.40	0.81	0.59	**This work**
Co@CNx	ORR||UOR	1.41	0.79	0.62	**This work**
Ni SAs-NC	ORR||UOR	1.39	0.85	0.54	[16]
Mn-$Ni(OH)_2$/CFC	ORR||UOR	1.30	0.60	0.70	[17]

Table S5. Comparison of Zn-air battery performances of $Co/CoSe_2$@CNx and other reported Co-based electrocatalysts.

Catalyst	Reactions	Specific capacity@j ($mAh\ g^{-1}$)	Energy conversion efficiency	Stability (h)	Ref.
$Co/CoSe_2$@CNx	ORR||OER	800@10	62.1%	140	**This work**
$CoSe_2$@NC	ORR||OER	751.1@10	54.1%	166	[6]
Co/CoSe@NC	ORR||OER	768.1@10	55.4%	125	[12]
Co-POC	ORR||OER	/	53.6 %	79	[18]
CoS/CoO@NGNs	ORR||OER	723.9@10	61.2%	100	[19]
Co_1-N_3PS/HC	ORR||OER	/	59.6 %	50	[20]
CoNi-SAs/NC	ORR||OER	750.9@20	55.2 %	79	[21]
Co_9S_8/Co-MCCNFs	ORR||OER	618.5@10	/	500	[22]

Supplementary References

1. Y. Zhao, C. Zhang, R. Fan, J. Li, Y. Hao, J. He, N. Alonso-Vante and J. Xue, *ChemElectroChem*, 2018, **5**, 3287-3292.
2. Z. Zeng, G. Fu, H. B. Yang, Y. Yan, J. Chen, Z. Yu, J. Gao, L. Y. Gan, B. Liu and P. Chen, *ACS Materials Letters*, 2019, **1**, 432-439.
3. J. Balamurugan, T. T. Nguyen, D. H. Kim, N. H. Kim and J. H. Lee, *Applied Catalysis B: Environmental*, 2021, **286**, 119909.
4. Y. Cao, S. Huang, Z. Peng, F. Yao, X. Li, Y. Liu, H. Huang and M. Wu, *Journal of Materials Chemistry A*, 2021, **9**, 3464-3471.
5. S.-H. Chae, A. Muthurasu, T. Kim, J. S. Kim, M.-S. Khil, M. Lee, H. Kim, J. Y. Lee and H. Y. Kim, *Applied Catalysis B: Environmental*, 2021, **293**, 120209.
6. K. Ding, J. Hu, J. Luo, W. Jin, L. Zhao, L. Zheng, W. Yan, B. Weng, H. Hou and X. Ji, *Nano Energy*, 2022, **91**, 106675.
7. S. Han, Y. Hao, Z. Guo, D. Yu, H. Huang, F. Hu, L. Li, H. Y. Chen and S. Peng, *Chemical Engineering Journal*, 2020, **401**, 126088.
8. Z. Qian, Y. Chen, Z. Tang, Z. Liu, X. Wang, Y. Tian and W. Gao, *Nano-Micro Letters*, 2019, **11**, 28.
9. T. Hu, Z. Jiang, Z. Fu and Z.-J. Jiang, *Journal of Materials Chemistry A*, 2022, **10**, 8739-8750.
10. G. Wang, J. Li, M. Liu, L. Du and S. Liao, *ACS Applied Materials & Interfaces*, 2018, **10**, 32133-32141.
11. K. Harish, J. Balamurugan, T. T. Nguyen, N. H. Kim and J. H. Lee, *Applied Catalysis B: Environmental*, 2022, **305**, 120924.
12. K. Li, R. Cheng, Q. Xue, P. Meng, T. Zhao, M. Jiang, M. Guo, H. Li and C. Fu, *Chemical Engineering Journal*, 2022, **450**, 137991.
13. N. Chen, Y.-X. Du, G. Zhang, W.-T. Lu and F.-F. Cao, *Nano Energy*, 2021, **81**, 105605.
14. Z. Liu, C. Zhang, H. Liu and L. Feng, *Applied Catalysis B: Environmental*, 2020, **276**, 119165.
15. C. Wang, X. Du and X. Zhang, *Journal of Alloys and Compounds*, 2022, **928**, 167094.
16. H. Jiang, J. Xia, L. Jiao, X. Meng, P. Wang, C.-S. Lee and W. Zhang, *Applied Catalysis B: Environmental*, 2022, **310**, 121352.
17. X. Zhang, G. Liu, C. Zhao, G. Wang, Y. Zhang, H. Zhang and H. Zhao, *Chemical Communications*, 2017, **53**, 10711-10714.
18. B. Q. Li, C. X. Zhao, S. Chen, J.-N. Liu, X. Chen, L. Song and Q. Zhang, *Advanced Materials*, 2019, **31**, 1900592.
19. Y. Tian, L. Xu, M. Li, D. Yuan, X. Liu, J. Qian, Y. Dou, J. Qiu and S. Zhang, *Nano-Micro Letters*, 2021, **13**, 3.
20. Y. Chen, R. Gao, S. Ji, H. Li, K. Tang, P. Jiang, H. Hu, Z. Zhang, H. Hao, Q. Qu, X. Liang, W. Chen, J. Dong, D. Wang and Y. Li, *Angewandte Chemie International Edition*, 2022, **61**, e202207879.
21. X. Han, X. Ling, D. Yu, D. Xie, L. Li, S. Peng, C. Zhong, N. Zhao, Y. Deng and

W. Hu, *Advanced Materials*, 2019, **31**, 1905622.
22. Z. Tang, Z. Nie, M. Yuan, Q. Lai and Y. Liang, *ChemElectroChem*, 2021, **8**, 3311-3317.